COMMUNICATIONS MATERIALS

ARTICLE

https://doi.org/10.1038/s43246-020-00048-4 OPEN

Selective phase growth and precise-layer control in $MoTe_2$

James P. Fraser[1], Liudvika Masaityte[1], Jingyi Zhang[2], Stacey Laing[3], Juan Carlos Moreno-López[4], Adam F. McKenzie[1], Jessica C. McGlynn[1], Vishal Panchal[5], Duncan Graham[3], Olga Kazakova[5], Thomas Pichler[4], Donald A. MacLaren[6], David A. J. Moran[2] & Alexey Y. Ganin[1✉]

Minor structural changes in transition metal dichalcogenides can have dramatic effects on their electronic properties. This makes the quest for key parameters that enable a selective choice between the competing metallic and semiconducting phases in the 2D $MoTe_2$ system compelling. Herein, we report the optimal conditions at which the choice of the initial seed layer dictates the type of crystal structure of atomically-thin $MoTe_2$ films grown by chemical vapour deposition (CVD). When Mo metal is used as a seed layer, semiconducting 2H-$MoTe_2$ is the only product. Conversely, MoO_3 leads to the preferential growth of metallic 1T′-$MoTe_2$. The control over phase growth allows for simultaneous deposition of both 2H-$MoTe_2$ and 1T′-$MoTe_2$ phases on a single substrate during one CVD reaction. Furthermore, Rhodamine 6G dye can be detected using few-layered 1T′-$MoTe_2$ films down to 5 nM concentration, demonstrating surface enhanced Raman spectroscopy (SERS) with sensitivity several orders of magnitude higher than for bulk 1T′-$MoTe_2$.

[1] School of Chemistry, University of Glasgow, Glasgow G12 8QQ, UK. [2] School of Engineering, University of Glasgow, Glasgow G12 8LT, UK. [3] Department of Pure and Applied Chemistry, University of Strathclyde, 99 George Street, Glasgow G1 1RD, UK. [4] University of Vienna, Faculty of Physics, Boltzmanngasse 5, A-1090 Vienna, Austria. [5] National Physical Laboratory, Teddington TW11 0LW, UK. [6] SUPA, School of Physics and Astronomy, University of Glasgow, Glasgow G12 8QQ, UK. ✉email: alexey.ganin@glasgow.ac.uk

Chemical vapour deposition (CVD) has become a key method for the universal growth of high-quality atomically thin transition metal dichalcogenides (TMDCs)[1–3]. Cheap in design and scalable to industry level, even in basic laboratory settings, a CVD apparatus holds promise for a wider acceptance of TMDCs in future applications. While MoS_2 and $MoSe_2$ few-layered films grown by CVD tend to invariably display only hexagonal structures, the less prominent $MoTe_2$ occurs in two polymorphic modifications[4]. The hexagonal (2H-$MoTe_2$) polymorph (Fig. 1a) in bulk form is an indirect-gap semiconductor but thinning it down to few-layers leads to the emergence of a direct bandgap of 1.1 eV[5]. This bandgap opening is accompanied by a strong photoluminescence signal in the near IR region (similar to Si), which makes 2H-$MoTe_2$ a viable candidate for optoelectronic devices[6–8]. Prototype photodetectors based on few-layered 2H-$MoTe_2$ have been suggested to become a future integrative part of silicon photonic applications[8–10]. Conversely, the monoclinic 1T′-$MoTe_2$ polymorph (Fig. 1b) is a Weyl semi-metal in the bulk form. Since the discovery of topological superconductivity and large magnetoresistance in this compound it has been the subject of comprehensive fundamental research[11–14]. In addition, 1T′-$MoTe_2$ has been highlighted as an emerging energy material with applications ranging from photovoltaic cells to hydrogen evolution catalysis[15–17]. Furthermore, few-layered 1T′-$MoTe_2$ may become a promising sensing platform enabled through its ability to suppress fluorescence signals which often prevents reliable detection of Raman scattering from negligible traces of molecules[18].

In this context, polymorphism in $MoTe_2$ presents an interesting opportunity to exploit the role of crystal structure on the electronic properties without the need for compositional change: a useful feature especially if the polymorphism can be controlled. However, unlike MoS_2 and $MoSe_2$[19,20], which rely on self-assembly by a van-der-Waals epitaxy (vdWE) process[21], the low electronegativity of Te presents a significant challenge for the deposition of atomically thin $MoTe_2$ by CVD. Despite the recent encouraging attempts[22,23], the tantalizing task of finding the ultimate set of empirically-determined parameters (gas flow rates, H_2/Ar ratio, substrate temperatures, heating/cooling rates), which can enable a controlled self-assembly of uniform and high-area $MoTe_2$ by vdWE remains elusive.

Direct tellurization CVD has emerged as a viable alternative to vdWE for achieving continuous and high-area growth of $MoTe_2$[24–27]. The process relies on a reaction (facilitated by the reductive flow of H_2) between Te vapour and an atomically thin seeding layer (commonly Mo-metal) pre-deposited on a substrate. However, the pronounced polymorphism in $MoTe_2$ makes the control of the reaction outcome extremely difficult. At deposition temperatures in excess of 600 °C (which are required for achieving high-quality products) both the semiconducting 2H-$MoTe_2$ and the semi-metallic 1T′-$MoTe_2$ polymorphs are in direct competition with each other at the substrate interface[22,28]. Through optimisation of reaction conditions it is possible to induce growth of a specific polymorph: for example, high ramping and cooling rates tend to produce 1T′-$MoTe_2$ while slower cooling rates and lower reaction temperatures generally lead to 2H-$MoTe_2$. However, this implies that the simultaneous growth of both 1T′-$MoTe_2$ and 2H-$MoTe_2$ would be impossible to achieve on the same substrate in a single step when the same seed layer is used. In practice, a post-growth modification, such as patterning, followed by a second CVD step is required[28,29]. Multiple-step procedures are unpractical from a future industrial applications point of view and therefore, finding a protocol for the preferential growth of both $MoTe_2$ polymorphs on the same substrate and through a single step procedure is important.

In this work, we report the growth of large-area and homogeneous films of few-layered 1T′- or 2H-$MoTe_2$ by CVD on SiO_2/Si and sapphire substrates using $FeTe_2$ precursor. At the deposition temperature of 650 °C the outcome of CVD is governed by the nature of the seeding layer with MoO_3 yielding 1T′-$MoTe_2$ and Mo leading to 2H-$MoTe_2$. This allows for the simultaneous growth of 1T′- and 2H-$MoTe_2$ to be achieved on the same substrate in a single step CVD reaction. The successful growth is evidenced by Raman spectroscopy, atomic force microscopy (AFM), X-ray photoelectron spectroscopy (XPS), transmission electron microscopy (TEM) and total colour difference microscopy techniques. Furthermore, few-layered films of the metallic 1T′-$MoTe_2$ phase shows sensing ability towards the detection of small molecules. Specifically, the common dye Rhodamine 6G (R6G) can be detected down to a 5 nM concentration on few-layered films, which is a significant improvement when compared with bulk 1T′-$MoTe_2$.

Results

CVD growth of few-layered 2H-$MoTe_2$ using Mo seeding layers. A CVD system (Fig. 1c) was designed and implemented to minimize the effect of the turbulence of the gas flow within the reactor and to keep the reaction conditions as close to equilibrium

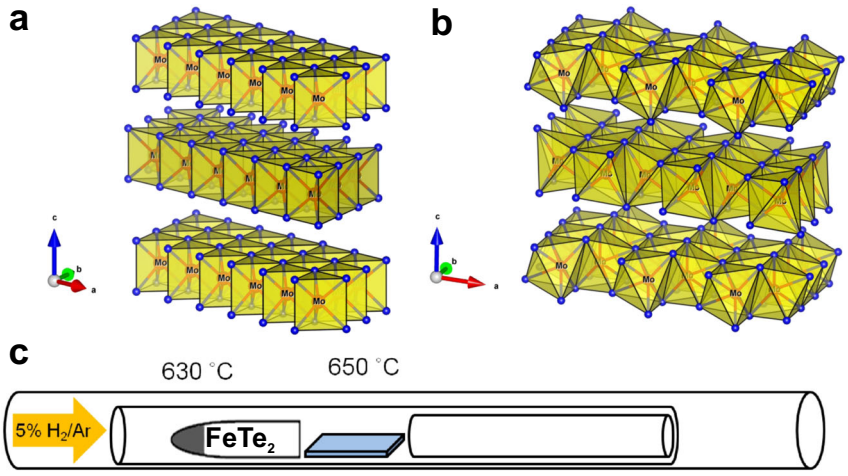

Fig. 1 Polymorphs of $MoTe_2$ and CVD setup. Crystal structure and polyhedral coordination of 3-layered hexagonal 2H-$MoTe_2$ (**a**) and monoclinic 1T′-$MoTe_2$ (**b**); A schematic of the CVD setup employed in this work (**c**). The temperatures of 630 °C and 650 °C stand for the temperature of the precursor source and substrate, respectively.

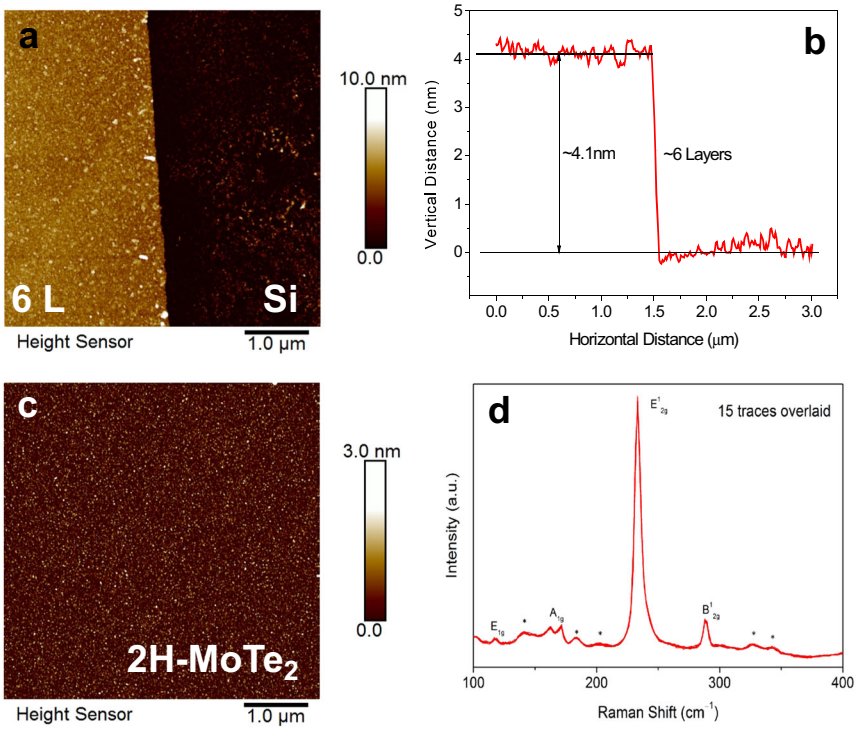

Fig. 2 Surface characterisation of 2H-$MoTe_2$ films. AFM measurement over the 5 μm × 5 μm area and a representative 2D topographic profile of the interface between few-layered 2H-$MoTe_2$ and SiO_2/Si substrate (**a**); the variation in height between the film and the substrate measured on a six-layered $MoTe_2$ film from Fig. 2a (**b**); 2D topographic profile of a 5 μm × 5 μm area from a few-layered $MoTe_2$ film on SiO_2/Si substrate (**c**); 532 nm Raman spectrum from a typical six-layered 2H-$MoTe_2$ on 300 nm SiO_2/Si (**d**).

as possible (see "Methods" section). $FeTe_2$ was selected as precursor due to a simple synthetic procedure, which involves reacting a stoichiometric mixture of Fe and Te powders in 5% H_2/Ar flow in a silica or alumina boat resulting in single phased $FeTe_2$ at 500 °C even without intermediate regrinding (Supplementary Fig. 1). Furthermore, according to TGA (Supplementary Fig. 2) the appreciable decomposition of $FeTe_2$ starts only above 600 °C. Therefore, the $FeTe_2$ precursor can be placed in close proximity to the substrate.

A typical AFM image of a $MoTe_2$ film obtained by conversion of a 1 nm thick Mo film (deposited by electron beam evaporation, see "Methods" Section) on a SiO_2/Si substrate at 650 °C using 30 mg $FeTe_2$ as a precursor is shown in Fig. 2a. The height profile collected at the step-edge between the film and the substrate corresponds to 4.1 nm (Fig. 2b). Based on the assumption that a monolayer of $MoTe_2$ should be *ca.* 0.7 nm thick (based on the length of the *c*-parameter in $MoTe_2$ according to synchrotron X-ray diffraction studies)[30] we estimated that the resulting film contains six $MoTe_2$ layers. A typical AFM image for this six-layered $MoTe_2$ across a scan area of 5 μm × 5 μm is shown in Fig. 2c. The measured root mean square surface roughness, R_q = 0.6 nm is in excellent agreement with the R_q = 0.6 nm observed on the initial 1 nm Mo film (Supplementary Fig. 3a). These roughness values are only marginally higher than that measured on a SiO_2/Si substrate with R_q = 0.45 nm (Supplementary Fig. 3b).

The in-plane E^1_{2g}-mode peak at *ca.* 234 cm^{-1} and a small out-of-plane A^1_g-mode peak at *ca.* 174 cm^{-1} in the Raman spectra of the film confirmed that the 2H-$MoTe_2$ polymorph is formed (Fig. 2d) while the wide range spectra confirmed that the films are free from MoO_3 and MoO_2 (Supplementary Fig. 4). The weak peaks at *ca.* 138 and 185 cm^{-1} are second-order Raman modes, as have been reported elsewhere[31]. The film is single-phase and uniform 2H-$MoTe_2$ across the entire substrate as evidenced from the perfect overlap of numerous spectra collected on the film at various locations across the substrate. Raman mapping based on the intensity of the E^1_{2g} mode also confirms the uniformity of the CVD grown film (Supplementary Fig. 5). In addition, the few-layered character of the grown 2H-$MoTe_2$ film was evident from the prominent phonon-active out-of-plane B^1_{2g} peak at *ca.* 289 cm^{-1} (Raman active in few-layered $MoTe_2$ but inactive in bulk).

The high-resolution XPS spectra of the six-layered 2H-$MoTe_2$ on SiO_2/Si exhibit spin-orbit doublets for two oxidation states (Supplementary Fig. 6a). The dominant doublet peaks at E_B = 228.12 eV and E_B = 231.2 eV can be assigned to Mo^{4+} $3d_{5/2}$ and Mo^{4+} $3d_{3/2}$ oxidation states for 2H-$MoTe_2$, respectively. The doublet upshifted to higher binding energies consists of a weak shoulder at E_B = 232.5 eV (Mo $3d_{5/2}$) and a broad feature at E_B = 235.71 eV (Mo $3d_{3/2}$), which are consistent with the binding energies expected for the molybdenum oxidation states in MoO_3[32,33]. The oxidation peaks have been reported in literature before and are probably due to minute surface oxidation in ambient air during transfer to the XPS[34]. The tellurium 3d spectrum displays a single doublet at E_B = 572.75 eV (Te $3d_{5/2}$) and E_B = 583.12 eV (Te $3d_{3/2}$) corresponding to $MoTe_2$ only (Supplementary Fig. 6b) suggesting that oxidation takes place only on Mo sites. In addition, by comparing our measurements with reference values[35], an upshift to higher binding energies of 0.12 eV for Mo $3d_{5/2}$ and a downshift of 0.35 eV for Te $3d_{5/2}$ peaks are observed, suggesting a net electron transfer from Mo to Te atoms. The rather moderate shift is in line with expectation given small differences in electronegativity between Mo and Te ($\Delta\chi_{Te\text{-}Mo}$ = 0.3). In the survey spectrum (Supplementary Fig. 6c), the Si peak arising from the substrate indicates that the beam penetrated through the entire film down to the SiO_2/Si substrate. That means the film is probed by XPS completely and since there is no evidence of Mo-metal peaks in the spectra, this suggests that the Mo seeding layer is completely converted into $MoTe_2$.

Transmission electron microscopy was used to assess the crystallinity of a six-layered film transferred onto Au grids (Supplementary Fig. 7a). The selected area electron diffraction confirmed the flake's polycrystallinity, which manifested as a sequence of diffraction rings rather than spots. At higher magnification the crystal structure is evident (Supplementary Fig. 7b), including a moiré fringe effect between crystal layers lying towards the centre of the image, and indicating a polycrystalline structure that is confirmed by a Fourier transform with multiple sets of hexagonal spots. Energy Dispersive X-ray Spectroscopy spectrum is dominated by Mo, Te and Au (support grid) peaks (Supplementary Fig. 8). Very weak Fe, C, Al and Si peaks are visible, at trace levels consistent with secondary scattering within the microscope which excludes any Fe-doping within the $MoTe_2$ films.

Since the spectroscopy and microscopy data confirmed the films grown on SiO_2/Si as uniform, single-phase 2H-$MoTe_2$, we additionally tested the method by growing $MoTe_2$ on a sapphire substrate. The positions and relative intensities of the peaks in the Raman spectra for the six-layers film grown on a sapphire substrate is similar with the films deposited on SiO_2/Si confirming the successful growth of semiconducting 2H-$MoTe_2$. However, the absolute peak intensities were found to be weaker relative to the base line (Supplementary Fig. 9) when compared with films on SiO_2/Si (Fig. 2d). For example, the peak associated with the E_{1g}-mode is unresolved due to the higher background. The subdued intensities are due to the transparency of the sapphire substrate to laser light[31], which is in line with the previous observations for a 2.1 nm $MoTe_2$ film obtained on sapphire by physical vapour deposition[36].

Controlled growth of 2H-$MoTe_2$ with different thicknesses. To the best of our knowledge all previous reports on $MoTe_2$ have been focused on one-off few-layered samples with only one report available where films with different thicknesses can be grown in the same CVD setup[37]. Therefore, we carried out the deposition process with the reaction parameters kept identical except for the thickness of the seeding Mo layer. Five Mo films with thicknesses of 0.75, 1, 1.25, 1.5 and 1.75 nm were deposited by thermal sputtering and then converted into $MoTe_2$.

The graph in Fig. 3a shows the correlation between the thicknesses of the initial Mo film and the thickness of the resulting $MoTe_2$ as measured by AFM. The relevant 2D topological AFM images of the interface between the films and the substrates are shown in Supplementary Fig. 10 while the height profiles for the films studied are summarized in Supplementary Fig. 11.

It is evident that the number of $MoTe_2$ layers (as before, under assumption that 1 $MoTe_2$ layer corresponds to *ca*. 0.7 nm) follows a clear trend line with the increase in the thickness of the initial Mo film. Conversely, there is no trend in the roughness of the films with increased thickness (Supplementary Fig. 12) suggesting that the produced films are similar in terms of their morphologies, as also can be seen from the 2D topographical images depending on film thicknesses (Supplementary Fig. 13). The AFM measurements confirmed that the samples at the studied thicknesses showed root mean square surface roughness (R_q) values below 1 nm, thus, indicating that the surfaces of the films were smooth and uniform and comparable with the original Mo seeding layer. The similarity of morphologies suggests an isomorphic transformation of the molybdenum layer into $MoTe_2$.

To test whether the same transformation can be achieved we carried out control CVD experiments by using elemental Te as source instead of $FeTe_2$. Changing $FeTe_2$ to Te leads to a different outcome of the reaction upon conversion of 1 nm Mo film to $MoTe_2$. From the optical microscopy the resulting product is visually inhomogeneous and discontinuous while the surface morphology appears to consist of grains or islands (Supplementary Fig. 14). The result is similar to a recent report that showed a substantial increase in the surface roughness of 2H-$MoTe_2$ compared with the initial Mo film when elemental Te was used[25]. We explain that the smooth surface of the films is retained when $FeTe_2$ is used due to slow heating and cooling rates of 5 °C min^{-1}, which are possible to apply due to the low vapour pressure of Te over the $FeTe_2$ precursor or/and lower Te^{2-} oxidation state. The slow rates may have helped to obtain smooth films by suppressing any differences in thermal coefficients between film and substrate, which would otherwise lead to rupturing of the film. It should be mentioned that in an attempt to test the suitability of $FeTe_2$ precursor for the growth of thicker films we converted 5 nm thick Mo seeding layer into $MoTe_2$ as well. Although the resulting films consisted solely of 2H-$MoTe_2$ there are unusual spots as evident from optical microscopy (Supplementary Fig. 15). Raman mapping was used to probe into nature of these spots which revealed that they consist of elevated islands of 2H-$MoTe_2$ as evident from the higher intensity of the E^1_{2g}-peak (Supplementary Fig. 15 insert).

Figure 3b shows the 532 nm laser Raman spectra collected on a range of 2H-$MoTe_2$ films with a different number of layers. Earlier work on exfoliated flakes of 2H-$MoTe_2$ has shown that the B^1_{2g}/E^1_{2g} peak intensity ratio could be a useful parameter for rapid evaluation of flake thickness as it correlates directly with the number of layers within 2H-$MoTe_2$[38]. Although the presence of the B^1_{2g} peak in Raman spectra of CVD-grown few-layered $MoTe_2$ films has been shown by various groups; to the best of our knowledge there are currently no reports where the B^1_{2g}/E^1_{2g} peak heights ratio *vs*. film thickness has been systematically investigated for CVD-grown few-layered $MoTe_2$ films. The B^1_{2g}/E^1_{2g} peak height intensity ratios depending on the film thickness are plotted in Fig. 3c. In addition, the analysis of the B^1_{2g} and E^1_{2g} peak positions (broadly following the B^1_{2g}/E^1_{2g} peak height ratio) is plotted in Fig. 3d showing that there is a distinctive trend with the film thickness. Both plots are in good agreement with layer thicknesses determined by AFM and collaborate well with the results based on available literature data for few-layered $MoTe_2$ obtained by mechanical exfoliation[38].

As the film thickness and number of $MoTe_2$ layers increases, the intensity of B^1_{2g} peak tends to decrease (Fig. 3d). However, there is a certain limitation for a simple evaluation of the number of layers by Raman spectroscopy: as the intensity of B^1_{2g} peak is getting suppressed, the B^1_{2g}/E^1_{2g} peak height ratio tends to plateau and becomes a relatively insensitive parameter for films with more than seven layers. We found that optical microscopy can be a useful tool for assessing thicker films (Supplementary Note 1). Therefore, we investigated the optical contrast difference (C_d) between the substrate (C_S) and the $MoTe_2$ film (C_F) by measuring the few-layered $MoTe_2$ samples using a cut-off filter (Supplementary Fig. 16). This procedure is similar to daylight illumination with the colour temperature of 6500 K equivalent to overcast daylight. As evident from the plot in Supplementary Fig. 16e, the splitting into R, B, G channels was necessary in order to see a trend with the thickness. The green channel tended to give the most reliable correlation between the optical contrast difference (C_d) for several films tested while blue and red channels saturated quite quickly. It is noteworthy that the optical microscopy appears to be a complementary technique for Raman spectroscopy as the C_d values continue an upward trend even when the number of layers is more than eight. The representative colour optical images showing the interface between the 300 nm SiO_2/Si substrate and all $MoTe_2$ films together with the

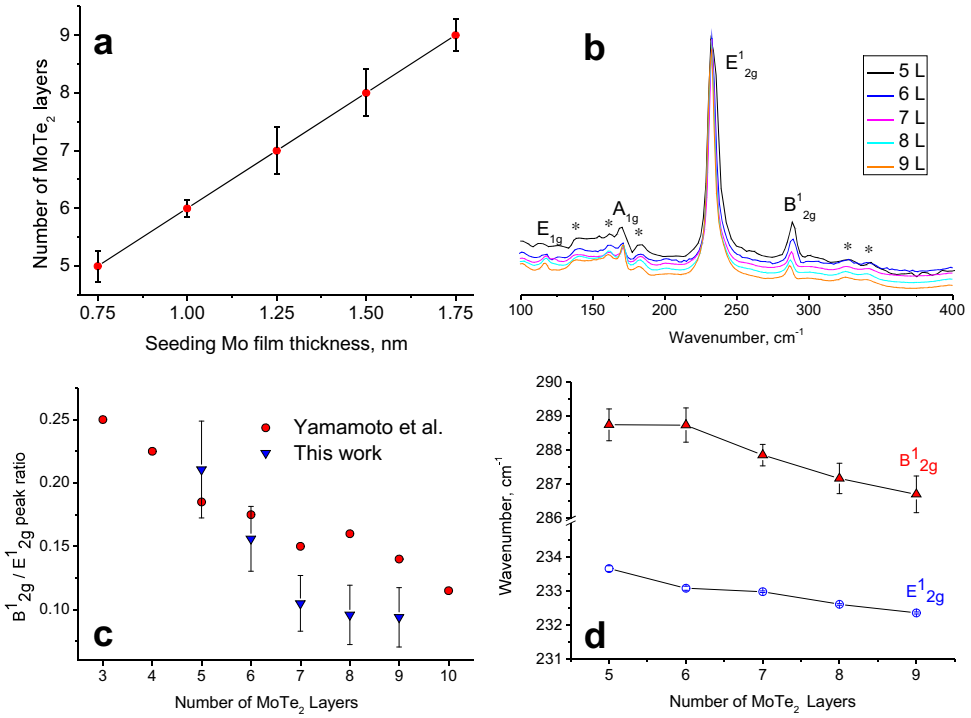

Fig. 3 The role of film thicknesses on Raman spectra. The correlation between the thickness of the thermally evaporated Mo film and the resulting few-layered $MoTe_2$ on 300 nm SiO_2/Si substrate. Errors are based on $n = 6$ independent points (**a**); 532 nm Raman spectra depending on number of layers in few-layered 2H-$MoTe_2$ on 300 nm SiO_2/Si substrates. The spectra are shifted along *y*-axis for clarity. The modes associated with 2H-$MoTe_2$ are labelled and second-order peaks are marked with asterisk (**b**); Raman data assessment of B^1_{2g}/E^1_{2g} ratio for $MoTe_2$ films on 300 nm SiO_2/Si depending on the number of layers (blue triangles). The data (red circles) for exfoliated $MoTe_2$ samples adopted from ref. [38]. are plotted for comparison. Errors are based on $n = 15$ independent points (**c**); Raman data assessment of the positions of B^1_{2g} and E^1_{2g} peaks depending upon the number of layers. Errors are based on $n = 15$ independent points (**d**).

corresponding grayscale images of RGB channels are summarized in Supplementary Fig. 17.

While the contrast between the substrate and the film tends to give quite good results in the case of CVD-grown films, it is not always possible or practical (for example, in upscale applications) to measure contrast in comparison with the substrate. However, 2H-$MoTe_2$ showed a tendency to have variation in colour depending on the number of layers. Therefore, we developed a practical colour palette, which could be used for a rapid assessment of the thicknesses of 2H-$MoTe_2$ films from optical microscopy (Supplementary Fig. 18). Depending on film thickness and nature of the irradiated light ranging from the "incandescent" 2300 K to "daylight" 6500 K there is a strong colour difference with the film thickness. Furthermore, using the intensity of the green channel we were able to produce a simple numerical plot which shows a very good correlation with the number of layers within $MoTe_2$ (Supplementary Fig. 16f).

Growth of few-layered 1T′-$MoTe_2$ using MoO_3 seeding layers. 1T′-$MoTe_2$ was grown within the same CVD setup and under identical reaction conditions as 2H-$MoTe_2$, except MoO_3 was used as a seeding layer instead of Mo. Figure 4a, b show a 2D topographic AFM image and the corresponding height profile collected at the step-edge between the $MoTe_2$ film and the substrate. The film thickness corresponds to four layers of $MoTe_2$ under the assumption of roughly 0.7 nm for one layer of $MoTe_2$. The thickness is comparable with the initial MoO_3 film (Supplementary Fig. 19). The roughness of the $MoTe_2$ ($R_q = 0.480$ nm) film (Fig. 4c) and initial thermally deposited MoO_3 ($R_q = 0.484$ nm) seeding layer (Supplementary Fig. 20) are identical when compared across scan areas of 5 μm × 5 μm. This indicates an isomorphic transformation of MoO_3 into $MoTe_2$ and suggests that the conversion is dictated by the quality of the initial seeding film and the reaction conditions are at optimal level.

Raman spectroscopy confirms that 1T′-$MoTe_2$ phase has been successfully grown[39], with several characteristic Raman peaks present between 50 and 400 cm^{-1}: A_g modes at ~80, ~108, ~125 and ~161 cm^{-1}, a B_g mode at ~186 cm^{-1} and two final A_g modes at 251 and 265 cm^{-1} respectively (Fig. 4d). The near identical peak positions and intensities of the peaks in the Raman spectra taken at 12 different locations across the film indicates the high-quality and uniformity of the 1T′-$MoTe_2$ films produced. Raman mapping based on the intensity of the characteristic A_g mode at 161 cm^{-1} reaffirms that the 1 T′-$MoTe_2$ films are uniform (Supplementary Fig. 21). Raman spectroscopy also reveals that the entire MoO_3 film was completely converted to $MoTe_2$ as the resulting spectra do not display any peaks associated with MoO_2 and MoO_3 (Supplementary Fig. 22).

The crystallinity of a 4-layered film was investigated using High Resolution Transmission Electron Microscopy (HRTEM) and Selected Area Electron Diffraction (SAED) as demonstrated in Supplementary Fig. 23. The data showed that the studied film was polycrystalline with the domain size of *ca.* 10 nm. However, the results are consistent with the recent literature report on 1 T′-$MoTe_2$ films grown at a similar temperature of 650 °C[27].

Simultaneous growth of 2H- and 1T′-$MoTe_2$. The phase selectivity of the reaction depending on the type of seeding layer used implies that there is an opportunity to exploit the difference in the outcome when Mo and MoO_3 seeding layers are used to grow both $MoTe_2$ polymorphs at the same time. Therefore, Mo and MoO_3 films on the same 300 nm SiO_2/Si substrate were converted

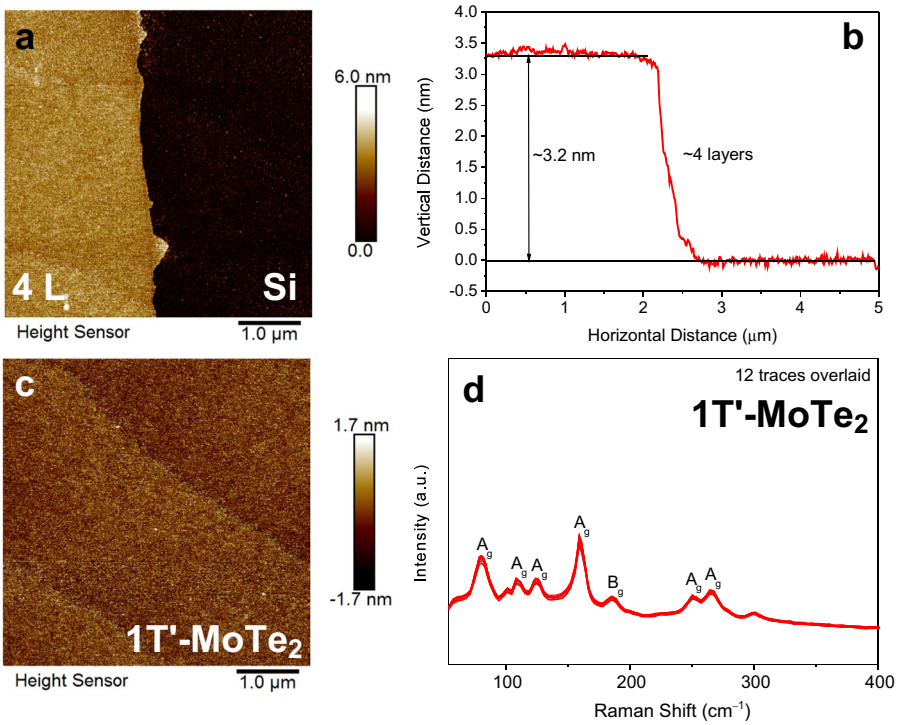

Fig. 4 Surface characterisation of 1T′-$MoTe_2$ films. AFM measurement over the 5 μm × 5 μm area and a representative 2D topographic profile of the interface between few-layered 1T′-$MoTe_2$ and SiO_2/Si substrate (**a**); the variation in height between the film and the substrate measured on a 4-layered 1T′-$MoTe_2$ film from Fig. 4a (**b**); 2D topographic profile of a 5 μm × 5 μm area of 4-layered $MoTe_2$ on SiO_2/Si substrate (**c**); 532 nm Raman spectrum from a typical four-layered 1T′-$MoTe_2$ on 300 nm SiO_2/Si (**d**).

using the same CVD setup and reaction conditions (650 °C and 30 mg of $FeTe_2$ precursor at the source). The successful simultaneous growth of phase pure 2H- and 1T′-$MoTe_2$ on the same substrate was confirmed by Raman spectroscopy with Mo converting to 2H-$MoTe_2$ and MoO_3 converting to 1T′-$MoTe_2$, respectively (Fig. 5a). An image taken from the sample shows the two phases separated by a 20-micron strip of bare SiO_2/Si substrate (Fig. 5b).

A careful assessment of the process was carried out by conducting the reactions at different flux rates, e.g. by using various amount of $FeTe_2$ at the source. The outcome of these studies is summarized in Supplementary Fig. 24. The simultaneous conversion of Mo to 2H-$MoTe_2$ and MoO_3 into 1 T′-$MoTe_2$ was achieved on the same substrate and in a single reaction at low loadings of $FeTe_2$ (30 mg). We hypothesise that the lower oxidation state of Te^{2-} in $FeTe_2$ leads to the simultaneous conversion at low evaporation rates due to 1T′-$MoTe_2$ phase being kinetically stabilized at the substrate[28]. In addition, we investigated the kinetics of reaction by varying CVD reaction times (1 s, 2 h, 4 h and 8 h) while keeping the amount of $FeTe_2$ fixed at 30 mg. Irrespective of reaction times the outcome was consistently 2H-$MoTe_2$ for Mo seeding layer and 1T′-$MoTe_2$ for MoO_3 seeding layer. Yoo et al.[28] pointed out that when formed the 1T′-$MoTe_2$ phase is kinetically stable at the substrate when Te vapour pressure is low which is the case for $FeTe_2$.

In order to understand why a specific phase is preserved depending on the seeding layer used we investigated the solid-to-solid transformation process by placing 5 mg MoO_3 and Mo powders on a Si/SiO_2 substrate within CVD apparatus in Fig. 1c. All experimental parameters were kept the same as the parameters used for the deposition of films. The reason for using powders was that even the shortest reaction time of 1 s was insufficient to identify the intermediate products in the case of thin films. Therefore, we hypothesised that using the bulk powders would allow us to achieve slower reaction rates and help us to identify the intermediate products. According to the Raman spectra in Supplementary Fig. 25a we identified that MoO_3 powder is first reduced to MoO_2 with no formation of $MoTe_2$ after a 4 h dwell while after 8 h of heating the spectrum is dominated by peaks belonging to 1 T′-$MoTe_2$. Conversely, Mo powder invariably converted to 2H-$MoTe_2$ irrespective of reaction time (Supplementary Fig. 25b). Based on these studies, we hypothesise that MoO_2 converts to 1T′-$MoTe_2$ preferentially because MoO_2 (same as 1T'-$MoTe_2$) has a low monoclinic crystal symmetry[40]. On the other hand, highly symmetrical cubic Mo metal tends to convert to higher crystal symmetry hexagonal 2H-$MoTe_2$ phase. Based on this assessment we added the reaction schematic for a mechanism of the reaction as a cartoon in Supplementary Fig. 26. Achieving simultaneous growth in a single reaction is an important development since the method proposed here does not rely upon any post-growth modification[28,29] and is only dependent upon the nature of initial Mo and MoO_3 seed layers, which are easy to control. Currently most methods for creating 1T′-2H junctions have focused on post-growth modification, involving techniques as varied as electrostatic doping, laser irradiation and the application of strain[28,41–43]. In this context, the access to a single step reaction may prove to be more advantageous and become widely adopted for future $MoTe_2$ applications.

Few-layered 1T′-$MoTe_2$ as a sensing substrate. A preliminary study was conducted to determine if few-layered 1T′-$MoTe_2$ films grown via CVD without any further modification could act as Surface Enhanced Raman Spectroscopy (SERS) substrates using a typical dye molecule, rhodamine 6G, as a Raman probe. The R6G solution (500 nM) was drop casted onto a film of 5-layer 1T′-$MoTe_2$ and a bare SiO_2/Si substrate before Raman spectra

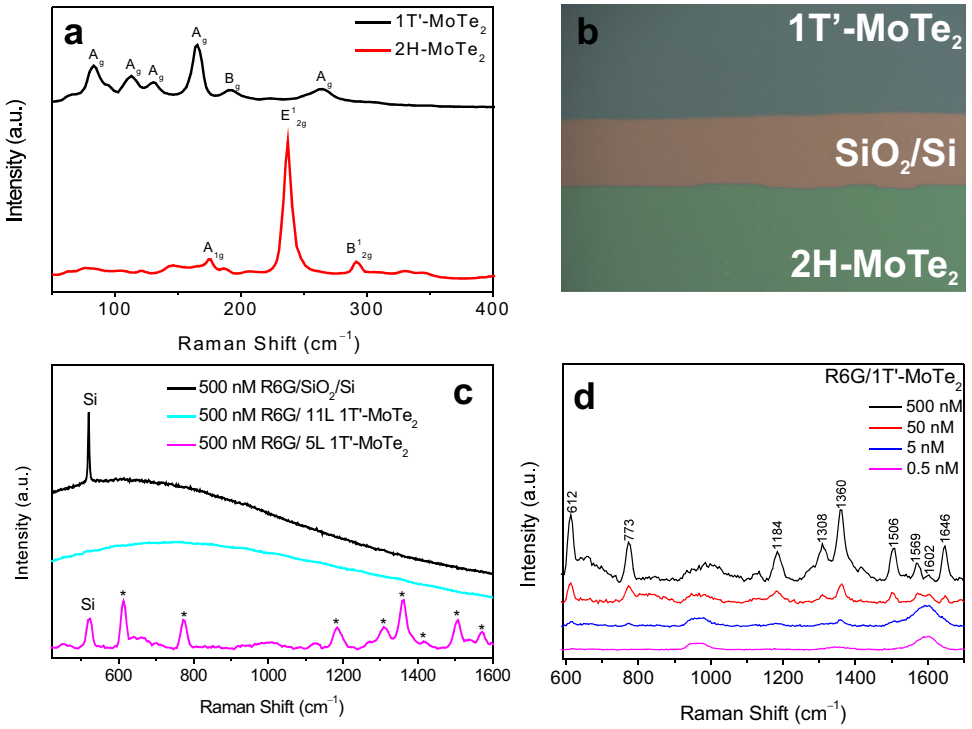

Fig. 5 One step growth of 1T′-$MoTe_2$ and 2H-$MoTe_2$ on a single substrate and SERS application of 1T′-$MoTe_2$. In all, 532 nm Raman spectra from 1T′- and 2H-$MoTe_2$ grown simultaneously on 300 nm SiO_2/Si substrate (**a**); an optical image of the two $MoTe_2$ phases grown simultaneously and separated by a ~20 μm strip of bare SiO_2/Si substrate for a better optical contrast (**b**); 532 nm Raman spectra of 500 nM solution of Rhodamine 6G drop casted on different substrates (**c**); concentration dependent 532 nm Raman studies of Rhodamine 6G spectra drop cast on the surface of 5 L 1T′-$MoTe_2$ film on SiO_2/Si substrate (**d**).

were collected from both areas (Fig. 5c and Supplementary Fig. 27 for wide range spectra). The signals collected from the R6G deposited on bare SiO_2/Si exhibit a large fluorescence background and no detectable Raman peaks for R6G can be found. In contrast to this, the fluorescence is massively suppressed by the 1T′-$MoTe_2$ film and Raman features of the dye, labelled with "*", are clearly visible. It is thought that the efficient charge transfer between $MoTe_2$ and R6G decreases the fluorescence cross section and causes subsequent fluorescence quenching[18]. The use of the few-layer 1T′-$MoTe_2$ film greatly increases the signal ratio of Raman/fluorescence features allowing for the R6G Raman peaks to be clearly distinguishable from the background. However, even at a relatively small increase in number of layers from 5-layered to 11-layered 1T′-$MoTe_2$ films resulted in the complete suppression of the SERS activity (Fig. 5c). Still, since 1T′-$MoTe_2$ does not have distinctive Raman modes (like phonon-active out-of-plane B^1_{2g} peak at *ca.* 289 cm^{-1} in 2H-$MoTe_2$) the sensing ability of few-layered samples towards R6G presents a good probe for distinguishing between atomically thin and bulk samples.

SERS is a technique routinely used to probe trace amounts of molecules; therefore, we tested the sensitivity of the technique. A set of R6G solutions were prepared with concentrations ranging from 500 to 0.5 nM to investigate the sensitivity of the SERS-active 1T′-$MoTe_2$ films. Figure 5d displays the Raman spectra of the R6G/1T′-$MoTe_2$ solutions depending on concentrations. Characteristic R6G Raman peaks at 612, 773, 1184, 1308, 1360, 1508, 1569, 1602 and 1646 cm^{-1} are labelled and are consistent with literature spectra. These peaks are clearly visible for the 500 and 50 nM concentrations. For the 5 nM solution it is possible to distinguish the peaks at 612, 773 and 1360 cm^{-1} from the background, but the peaks within the 1569–1646 cm^{-1} range exhibit a significant broadening and it is no longer possible to distinguish these peaks individually. Below this concentration, individual peaks cannot be identified. Recent studies on the use of 2D materials as SERS substrates show that the enhancement factor is highly dependent upon the thickness of the 2D material[44–46]. Decreasing the thickness of a substrate leads to increasing enhancement factors.

Discussion

In conclusion, we have described a viable method which is suitable for achieving preferential growth of two stable $MoTe_2$ polymorphs on the same substrate and in a single reaction. We have also demonstrated the applicability of a $FeTe_2$ precursor for the preparation of a desired polymorph under controlled conditions. In this context, the recent advancement in nanolithography technology provides the opportunity to design seeding layers to a high level of precision before the CVD process. Therefore, a single step route to the growth of a preferred $MoTe_2$ polymorph where the outcome of a CVD reaction is dictated solely by the composition of the seeding layer can help the progress in rational and reproducible design of $MoTe_2$-based systems. Hence, this method may help to advance the adaptability of 2D chalcogenides in practical applications, such as the phase-controlled growth of metallic/semiconducting coplanar homojunctions.

Methods

Synthesis. Substrates were cut using a diamond tipped scribe from a wafer of 300 nm SiO_2/Si (100) (Inseto) to a size of 10 × 10 mm^2. Smaller 8 × 8 mm^2 were diced using a diamond saw. The substrates were cleaned via ultrasonication in acetone and isopropyl alcohol, spending 10 minutes in each solvent before being dried in a stream of nitrogen gas.

Specified thicknesses of molybdenum (99.95%) were deposited on to the cleaned substrates via electron beam physical vapour deposition using a Plassys MEB550s. Deposition occurred under a vacuum of 1 × 10^{-6} mbar at a rate of 0.07 nm s^{-1}, with the electron beam gun emission current at 220 mA. The thicknesses of the molybdenum films were controlled by a quartz crystal microbalance. MoO_3

films were deposited by thermal evaporation of MoO_3 pellets (99.99%, Pi-Kem) in a Plassys MEB400 under a vacuum of 2×10^{-6} mbar and at a rate of 0.2 nm/s.

Chemical vapour deposition was used to synthesise the $MoTe_2$ thin films. Firstly, into a 31.5 cm quartz ampoule (inside diameter: 12 mm, outside diameter: 15 mm) was placed a 13.5 cm quartz tube (inside diameter: 9 mm, outside diameter: 11 mm) until it was resting against the end of the larger ampoule. Then the substrate was placed into the quartz ampoule until it rested against the quartz tube. Subsequently 30–33 mg of $FeTe_2$ powder was placed into a 7 cm long quartz ampoule (inside diameter: 9 mm, outside diameter: 11 mm), which was inserted into the large quartz ampoule until the open end rested against the substrate. The 31.5 cm ampoule was placed into a 43.5 cm quartz work tube (inside diameter: 17 mm, outside diameter: 20 mm) which itself resides inside a Lenton tube furnace. One end of the work tube was connected to a cylinder of 5% H_2/Ar carrier gas, whilst the other end was connected to a vacuum pump through which the system could be evacuated. Before the CVD process began the system was evacuated to a pressure of 2×10^{-1} mbar, before being refilled with the carrier gas, this procedure was carried out a total of three times to ensure an oxygen free environment for the reaction. The substrate temperature was set to 650 °C and source temperature with $FeTe_2$ precursor at 630 °C. The ramping rate was at 5 °C min^{-1} with a dwell time of 4 h, before cooling to room temperature at 5 °C min^{-1}. A commercially available and safe carrier gas mixture containing only 5 vol. % of H_2 in Ar was used at a flow rate of 300 sccm.

Characterisation. Raman measurements were carried out in a backscattering configuration on a Horiba-JY HR800 spectrometer equipped with a solid-state green laser ($\lambda = 532$ nm). All spectra were collected unless otherwise stated through a 50× objective and dispersed by 1200 g mm^{-1} grating. The Si and sapphire most intense peaks were used as internal standards. The laser power used to irradiate samples was kept at 10 mW to avoid sample degradation and the diameter of the confocal pinhole was 100 µm.

Raman maps were measured on a WITec alpha300 R spectrometer using a 532 nm laser excitation. Spectra were collected using a 50× objective with a 1-s integration time and 1 µm spatial resolution. Background subtraction of the spectra was carried out on WITec Project 4.1 software and maps were generated based on the intensity of the peaks.

XPS spectra were collected on a system consisting of a Scienta MX650 ×-ray source coupled with a Scienta RS4000 hemispherical analyser. XPS spectra were acquiring using a monochromatic Al *Kα* anode (photon energy = 1486.7 eV) with a pass energy of 200 eV in the hemispherical analyser. The XPS set-up was kept at a pressure of 1×10^{-9} mbar and samples were attached to a copper holder and annealed at 300 °C under vacuum for an hour before XPS spectra were recorded to remove surface contaminants.

Transmission electron microscopy was conducted on a JEOL CFEG ARM instrument operated at 200 kV, using samples supported by holey carbon films and Au grids. Selected area electron diffraction patterns were typically collected from a 20 or 50 micrometre diameter area. Beam damage was evident for the 1T′ samples but not for the 2H sample after prolonged exposure to the electron beam. To remove $MoTe_2$ films from SiO_2/Si substrates, they were submersed in 10% HF solution for ~30 s before being placed into a beaker filled with deionised water so that the $MoTe_2$ films floated on the surface. The films were then scooped up with Carbon on 200 mesh grids. Energy dispersive X-ray spectroscopy (EDS) data was collected in (probe-corrected) scanning transmission electron microscopy mode, employing a Bruker X-Flash detector.

AFM measurements were obtained using a Bruker Dimension Icon AFM. Film steps relative to the SiO_2/Si substrate were measured over a scan area of 5 µm × 5 µm. The step edges were created by using a permanent marker to draw a line ~2 mm wide across a bare SiO_2/Si substrate. Subsequently molybdenum was deposited onto the substrate, before being sonicated in isopropyl alcohol for 30 s to remove the marker, taking a ~2-mm thick line of molybdenum with it, hence leaving a bare area of SiO_2/Si adjacent to the deposited molybdenum film. The molybdenum film was then converted to $MoTe_2$ using the procedure described above, allowing the $MoTe_2$ film thickness to be measured against the bare line of SiO_2/Si substrate. Surface roughness measurements were also recorded over a scan area of 5 µm × 5 µm for SiO_2/Si substrate, Mo, MoO_3 and $MoTe_2$ films. A new tip was used for each sample to minimise errors associated with the AFM instrument.

Olympus BX41 microscope integrated in Horiba-JY HR800 spectrometer was used for optical imaging. All images were captured using 50× objective. Intensity of the light source (Euromex fiber optic light source EK-1, equipped with 12 V, 100 W halogen lamp) was adjusted to level 8 when capturing images for contrast measurements and to level 8.5 when capturing images for the colour palette. White balance was adjusted to R: $B = 0.91$: 1.21 via the source settings section in LabSpec5 software when capturing contrast images. White balance was adjusted to imitate different colour temperature white light sources when capturing images for the colour palette.

Optical contrast difference was measured using ImageJ software. Colour optical images were split into RGB channels using "Split Channels" function. Contrast profile was obtained by selecting an area in the image and then pressing "K".

SERS measurements. R6G was diluted to 10 mM in ethanol, followed by subsequent dilution to the desired concentration in water. A 10 µL spot of diluted R6G was applied to the surface and left to dry before a gentle rinse with water and subsequent drying. SERS spectra were obtained on a WITec alpha 300R with a 532 nm laser excitation wavelength (laser power at sample 33 mW) and a 600 g mm^{-1} diffraction grating. Spectra were acquired using a 10× objective with a 1-s integration time. Spectra averaging (of 3 spectra per sample) and baseline subtraction was carried out in WiRE 4.2 software.

Data availability

The data sets generated during the current study are available from the corresponding authors upon reasonable request.

Received: 26 March 2020; Accepted: 25 June 2020;
Published online: 24 July 2020

References

1. Manzeli, S., Ovchinnikov, D., Pasquier, D., Yazyev, O. V. & Kis, A. 2D transition metal dichalcogenides. *Nat. Rev. Mater* **2**, 17033 (2017).
2. Zhou, J. et al. A library of atomically thin metal chalcogenides. *Nature* **556**, 355–359 (2018).
3. Zhang, Y. et al. Recent progress in CVD growth of 2D transition metal dichalcogenides and related heterostructures. *Adv. Mater.* **31**, 1901694 (2019).
4. Brown, B. E. The crystal structures of WTe 2 and high-temperature $MoTe_2$. *Acta Crystallogr.* **20**, 268–274 (1966).
5. Keum, D. H. et al. Bandgap opening in few-layered monoclinic $MoTe_2$. *Nat. Phys.* **11**, 482–486 (2015).
6. Reeves, L., Wang, Y. & Krauss, T. F. 2D material microcavity light emitters: to lase or not to lase? *Adv. Opt. Mater.* **6**, 1800272 (2018).
7. Li, A. et al. Ultrahigh-sensitive broadband photodetectors based on dielectric shielded $MoTe_2$/Graphene/SnS_2 p–g–n junctions. *Adv. Mater.* **31**, 1805656 (2018).
8. Bie, Y. Q. et al. A $MoTe_2$-based light-emitting diode and photodetector for silicon photonic integrated circuits. *Nat. Nanotechnol.* **12**, 1124–1129 (2017).
9. Fang, H. et al. 1305 nm few-layer $MoTe_2$-on-silicon laser-like emission. *Laser Photonics Rev.* **12**, 1800015 (2018).
10. Fang, H. et al. Laser-like emission from a sandwiched $MoTe_2$ heterostructure on a silicon single-mode resonator. *Adv. Opt. Mater.* **7**, 1900538 (2019).
11. Qi, Y. et al. Superconductivity in Weyl semimetal candidate $MoTe_2$. *Nat. Commun.* **7**, 11038 (2016).
12. Yan, B. & Felser, C. Topological materials: weyl semimetals. *Annu. Rev. Condens. Matter Phys.* **8**, 337–354 (2017).
13. Jiang, J. et al. Signature of type-II Weyl semimetal phase in $MoTe_2$. *Nat. Commun.* **8**, 13973 (2017).
14. Yuan, S. et al. Room-temperature ferroelectricity in $MoTe_2$ down to the atomic monolayer limit. *Nat. Commun.* **10**, 1775 (2019).
15. Hussain, S. et al. Large area growth of $MoTe_2$ films as high performance counter electrodes for dye-sensitized solar cells. *Sci. Rep* **8**, 29 (2018).
16. McGlynn, J. C. et al. The rapid electrochemical activation of $MoTe_2$ for the hydrogen evolution reaction. *Nat. Commun.* **10**, 4916 (2019).
17. Zhuang, P. et al. Revisiting the role of active sites for hydrogen evolution reaction through precise defect adjusting. *Adv. Funct. Mater.* **29**, 1901290 (2019).
18. Tao, L. et al. 1T′ transition metal telluride atomic layers for plasmon-free SERS at femtomolar levels. *J. Am. Chem. Soc.* **140**, 8696–8704 (2018).
19. Cain, J. D., Shi, F., Wu, J. & Dravid, V. P. Growth mechanism of transition metal dichalcogenide monolayers: the role of self-seeding fullerene nuclei. *ACS Nano* **10**, 5440–5445 (2016).
20. Li, S. et al. Vapour-liquid-solid growth of monolayer MoS_2 nanoribbons. *Nat. Mater.* **17**, 535–542 (2018).
21. Kim, J. et al. Principle of direct van der Waals epitaxy of single-crystalline films on epitaxial graphene. *Nat. Commun.* **5**, 4836 (2014).
22. Zhou, J. et al. Large-area and high-quality 2D transition metal telluride. *Adv. Mater.* **29**, 1603471 (2017).
23. Sung, J. H. et al. Coplanar semiconductor-metal circuitry defined on few-layer $MoTe_2$ via polymorphic heteroepitaxy. *Nat. Nanotechnol* **12**, 1064–1070 (2017).
24. Zhou, L. et al. Synthesis of high-quality large-area homogenous 1T′ $MoTe_2$ from chemical vapor deposition. *Adv. Mater.* **28**, 9526–9531 (2016).
25. Zhou, L. et al. Role of molecular sieves in the CVD synthesis of large-area 2D $MoTe_2$. *Adv. Funct. Mater.* **27**, 1603491 (2017).
26. Yun, S. J. et al. Telluriding monolayer MoS_2 and WS_2 via alkali metal scooter. *Nat. Commun.* **8**, 2163 (2017).
27. Xu, X. et al. Millimeter-scale single-crystalline semiconducting $MoTe_2$ via solid-to-solid phase transformation. *J. Am. Chem. Soc.* **141**, 2128–2134 (2019).

28. Yoo, Y., DeGregorio, Z. P., Su, Y., Koester, S. J. & Johns, J. E. In-plane 2H-1T′ $MoTe_2$ homojunctions synthesized by flux-controlled phase engineering. *Adv. Mater.* **29**, 1605461 (2017).
29. Ma, R. et al. $MoTe_2$ lateral homojunction field-effect transistors fabricated using flux-controlled phase engineering. *ACS Nano* **13**, 8035–8046 (2019).
30. McGlynn, J. C. et al. Molybdenum ditelluride rendered into an efficient and stable electrocatalyst for the hydrogen evolution reaction by polymorphic. *Control. Energy Technol.* **6**, 345–350 (2018).
31. Ruppert, C., Aslan, O. B. & Heinz, T. F. Optical properties and band gap of single- and few-layer MoTe2 crystals. *Nano Lett.* **14**, 6231–6236 (2014).
32. Fleisch, T. H. & Mains, G. J. An XPS study of the UV reduction and photochromism of MoO_3 and WO_3. *J. Chem. Phys.* **76**, 780–WO786 (1982).
33. Plyuto, Y. V., Babich, I. V., Plyuto, I. V., Van Langeveld, A. D. & Moulijn, J. A. XPS studies of MoO_3/Al_2O_3 and MoO_3/SiO_2 systems. *Appl. Surf. Sci.* **119**, 11–18 (1997).
34. Naylor, C. H. et al. Monolayer single-crystal 1T′-$MoTe_2$ grown by chemical vapor deposition exhibits weak antilocalization effect. *Nano Lett.* **16**, 4297–4304 (2016).
35. Wagner, C. D. *Handbook of x-ray photoelectron spectroscopy: a reference book of standard data for use in x-ray photoelectron spectroscopy, Physical Electronics Division, Perkin-Elmer Corp*. (Physical Electronics Division Perkin-Elmer Corp., 1979).
36. Huang, J. H. et al. Large-area 2D layered $MoTe_2$ by physical vapor deposition and solid-phase crystallization in a tellurium-free atmosphere. *Adv. Mater. Interfaces* **4**, 1700157 (2017).
37. Cui, J. et al. Transport evidence of asymmetric spin–orbit coupling in few-layer superconducting $1T_d$-$MoTe_2$. *Nat. Commun.* **10**, 1–8 (2019).
38. Yamamoto, M. et al. Strong enhancement of Raman scattering from a bulk-inactive vibrational mode in few-layer $MoTe_2$. *ACS Nano* **8**, 3895–3903 (2014).
39. Zhou, L. et al. Sensitive phonon-based probe for structure identification of 1T′ $MoTe_2$. *J. Am. Chem. Soc.* **139**, 8396–8399 (2017).
40. Bolzan, A. A., Kennedy, B. J. & Howard, C. J. Neutron powder diffraction study of molybdenum and tungsten dioxides. *Aust. J. Chem.* **48**, 1473–1477 (1995).
41. Cho, S. et al. Phase patterning for ohmic homojunction contact in $MoTe_2$. *Science* **349**, 625–628 (2015).
42. Song, S. et al. Room temperature semiconductor-metal transition of $MoTe_2$ thin films engineered by strain. *Nano Lett.* **16**, 188–193 (2016).
43. Wang, Y. et al. Structural phase transition in monolayer $MoTe_2$ driven by electrostatic doping. *Nature* **550**, 487–491 (2017).
44. Qiu, C. et al. Investigation of *n* -Layer graphenes as substrates for raman enhancement of crystal violet. *J. Phys. Chem. C* **115**, 10019–10025 (2011).
45. Ling, X. et al. Raman enhancement effect on two-dimensional layered materials: Graphene, h-BN and MoS_2. *Nano Lett.* **14**, 3033–3040 (2014).
46. Lee, Y. et al. Enhanced raman scattering of rhodamine 6G Films on two-dimensional transition metal dichalcogenides correlated to photoinduced charge transfer. *Chem. Mater.* **28**, 180–187 (2016).

Acknowledgements

We acknowledge the University of Glasgow, EPSRC (EP/P001653/1 and EP/N509668/1), and the Carnegie Trust for a Research Incentive Grant (RIG007428) for supporting this work. T.P. thanks the FWF P27769-N20 for funding. J.P.F thanks the Energy Technology Partnership for the PECRE grant awarded. The work at NPL has been financially supported by the EU Graphene Flagship under grant agreement GrapheneCore3 881603 and the Department for Business, Energy and Industrial Strategy through NMS funding (2D Materials Cross-team project).

Author contributions

A.G. directed and coordinated the project. J.P.F. and A.G. designed the experiments. J.P.F., L.M. and A.M. carried out CVD experiments. J.P.F., L.M., J.Z., V.P. collected and interpreted Raman, optical microscopy and AFM data with help of A.G., O.K., T.P. and D.A.J.M. J.C.M.L. and J.P.F. collected and interpreted XPS data with help of T.P. J.C.M. and J.P.F. synthesised and characterised $FeTe_2$ precursor. D.A.M. carried out and evaluated HRTEM experiments. S.L. carried out SERS studies with help of D.G. J.P.F. and A.G. wrote the paper. All authors commented on the paper.

Competing Interests

The authors declare no competing interests.

Additional information

Supplementary information is available for this paper at https://doi.org/10.1038/s43246-020-00048-4.

Correspondence and requests for materials should be addressed to A.Y.G.

Reprints and permission information is available at http://www.nature.com/reprints

Publisher's note Springer Nature remains neutral with regard to jurisdictional claims in published maps and institutional affiliations.